THE ROLE OF BLACK-BOX MODELS IN ROTORCRAFT ATTITUDE CONTROL

Marco Bergamasco **Nicola Cortigiani** **Diego Del Gobbo**
Leonardo Helicopter Division, Italy
{marco.bergamasco02,nicola.cortigiani,diego.delgobbo}@leonardocompany.com

Simone Panza **Marco Lovera**
Dipartimento di Scienze e Tecnologie Aerospaziali, Politecnico di Milano, Italy
{simone.panza,marco.lovera}@polimi.it

Abstract: Black-box model identification methods of the subspace class can provide more accurate multivariable continuous-time state-space models with respect to frequency-domain procedures applied to structured models. The use of black-box models, however, comes with a number of issues, which have to be addressed to successfully employ them in the control design toolchain: the aim of this paper is to discuss the main issues which have to be dealt with before the raw black-box models can be effectively employed for control law design.

1. INTRODUCTION

Helicopter attitude control law design is a very challenging problem, as helicopters exhibit open-loop unstable, non-minimum phase, intrinsically multivariable attitude responses, to which tight stability and performance requirements must be imposed. The complexity of the design problem is further increased by the difficulty of accurately capturing attitude dynamics with physical models: as is well known, while direct attitude responses can be reasonably well represented by first-principles models, cross-terms in the attitude dynamics could not be captured with sufficient accuracy for control purposes. The above discussion motivates the significant interest in rotorcraft model identification over the last few decades, which has led to the development of numerous dedicated methods and tools, both in the time-domain and in the frequency-domain (see for example the recent books[1,2] and the references therein).

Most of the existing rotorcraft model identification literature focuses on the estimation of the parameters of physically-motivated model structures, *i.e.*, stability and control derivatives and time delays in linearised flight dynamics models. While this approach has some advantages as it may lead to gathering some physical insight from the obtained models, the fact that the model structure is fixed is a loss of flexibility in the identification procedure, which might turn out as a performance penalty with respect to black-box methods. Indeed, it has been shown[3] that black-box methods of the Subspace Model Identification (SMI) class[4,5] can provide more accurate multivariable continuous-time state-space models with respect to frequency-domain procedures applied to structured models. Currently, continuous-time black-box models identified using subspace methods[3] are being successfully used at Leonardo Helicopters for the assessment of the Automatic Flight Control System (AFCS) and for the dynamics validation of nonlinear physical models (see also the companion paper[6]).

The use of black-box models, however, comes with a number of issues, which have to be addressed to successfully employ them in the control design toolchain: the aim of this paper is to discuss the main issues which have to be dealt with before the raw black-box models can be effectively employed for control law design. More precisely, the following points will be addressed and illustrated using models identified for Leonardo helicopter prototypes:

- Uncertainty modelling: the uncertainty of the identified models has to be quantified. The analysis of the asymptotic variance for subspace methods has been widely discussed in the literature[7] and both explicit expressions and computational approaches to the problem of evaluating model uncertainty have been developed[8].
- Analysis of black-box models: the identified models have to be analysed to check that they do not contain modes introduced by numerical artifacts. Such a verification is mainly carried out in terms of classical modal analysis. Similarly, the output equation has to be inspected to check the elements of the direct feed-through term D, which is returned by the identification procedure but which is likely to be non-physical.
- Physical interpretation of black-box models: the main downside of subspace methods is that they return state-space models in which the state variables cannot be given a physical interpretation.

However, a state transformation can be constructed such that the output variables have a one-to-one dependency on the state variables, *i.e.*, the output matrix is the identity matrix or a partition of the identity matrix.

2. BLACK-BOX ROTORCRAFT MODEL IDENTIFICATION

The theory of MIMO linear systems was already completely understood by the late 70s[9], and yet from a practical point of view black-box identification of MIMO systems remained an issue until the late 80s. The cause for this was the estimation of the structural indices that characterize the parameterizations of MIMO systems, which is tricky and often leads to ill-conditioned numerical problems[10]. SMI methods offered exactly the potential to overcome this difficulty: classical SMI methods, developed in the early 90s for the estimation of discrete-time models[11,12] allowed for the first time to deal with MIMO problems in an effective way, thanks to the simple and non-iterative implementation. Extensions to continuous-time systems followed a few years later[13,14] and more recently methods capable of dealing with data collected in closed-loop (as is typically the case in rotorcraft applications[2,15,1]) were developed as well, both for discrete-time[16] and continuous-time[4].

The problem of continuous-time black-box state-space model identification can be concisely stated as follows, with reference to the linear, time-invariant continuous-time model

$$\begin{aligned} \dot{x}(t) &= Ax(t) + Bu(t) + w(t),\ x(0) = x_0 \\ y(t) &= Cx(t) + Du(t) + v(t) \end{aligned} \tag{1}$$

where $x \in \mathbb{R}^n$, $u \in \mathbb{R}^m$ and $y \in \mathbb{R}^p$ are, respectively, the state, input and output vectors and $w \in \mathbb{R}^n$ and $v \in \mathbb{R}^p$ are the process and the measurement noise, respectively, with covariance given by

$$E\left\{ \begin{bmatrix} w(t_1) \\ v(t_1) \end{bmatrix} \begin{bmatrix} w(t_2) \\ v(t_2) \end{bmatrix}^T \right\} = \begin{bmatrix} Q & S \\ S^T & R \end{bmatrix} \delta(t_2 - t_1).$$

Note that in this setting the input u and the noise process w,v are not required to be incorrelated, so that data collected under feedback can be used without incurring any bias in the estimates. The system matrices A, B, C and D are such that (A, C) is observable and $(A, [B, Q^{1/2}])$ is controllable. One or more datasets $\{u(t_i), y(t_i)\}_j$, $i \in [1, N]$, $j \in [1, K]$ of sampled input/output data (possibly associated with a non equidistant sequence of sampling instants) obtained from the true system are available.

Then, the problem is to provide estimates of the state space matrices A, B, C and D (up to a similarity transformation) on the basis of the available data. The model identification algorithm considered herein is the Continuous-Time Predictor-Based Subspace IDentification (CT-PBSID) method, which uses time-domain data to compute a black-box estimate of a linear state-space model in the form (1). A detailed presentation of CT-PBSID can be found in previous publications[4]; in this paper only a concise description of the algorithm is provided:

- the time-domain data is converted to the Laguerre domain by means of the transformations

$$\begin{aligned} \tilde{u}(k) &= \int_0^\infty \ell_k(t) u(t) dt \\ \tilde{y}(k) &= \int_0^\infty \ell_k(t) y(t) dt \end{aligned} \tag{2}$$

  where $\tilde{u}(k) \in \mathbb{R}^m$, $\tilde{y}(k) \in \mathbb{R}^p$ and $\ell_k(t)$ is the impulse response of the k-th Laguerre filter, defined as

$$\mathcal{L}_k(s) = \sqrt{2a} \frac{(s-a)^k}{(s+a)^{k+1}}. \tag{3}$$

- Using the transformed data, algebraic data equations are formed, to represent the input-output behaviour over a 'past' horizon p and a 'future' horizon f (in terms of the index k, now interpreted as a discrete-time index).

- From the data equations an estimate of the model order and of the state sequence of the system over the future horizon can be computed.

- Finally, the state space representation of the system in the discrete-time k can be estimated and the original continuous-time dynamics is recovered.

The obtained state-space black-box models, however, come with a number of issues, described in the Introduction, which have to be addressed to employ them in the control design toolchain. Approaches to each of these issues will be illustrated in the following sections.

3. UNCERTAINTY MODELLING

Classical parameter estimation methods based on the maximum likelihood principle provide information about the asymptotic variance of the estimates in terms of the Cramer-Rao bound (see for example[15]). Similarly, the analysis of the asymptotic variance for subspace identification methods has been widely discussed in the literature (see, *e.g.*,[7] and the references therein) and explicit expressions for it have been worked out. In a parallel development, a computationally viable approach to the problem of evaluating the uncertainty of models identified using subspace

algorithms (both for discrete-time and continuous-time models) has been developed, in which the bootstrap is employed to evaluate the standard deviation of invariants of the estimated models, such as the eigenvalues and the frequency response functions[8]. Such uncertainty information can be combined with uncertainty estimates associated with nonparametric frequency response function estimates to develop control-oriented uncertainty model structures.

In this Section a bootstrap-based procedure[17] for the evaluation of the uncertainty associated with invariants such as the frequency response of the estimated models is illustrated. The bootstrap is a computational statistical method which can solve the following problem: given a random, independent, identically distributed (i.i.d.) sample $\mathbf{x} = (\mathbf{x_1}, \mathbf{x_2}, \ldots, \mathbf{x_n})$ drawn from an unknown distribution F, one computes an estimate $\hat{\theta}$ of the parameter $\theta = t(F) = t[\mathbf{x}]$ on the basis of the available data, and would like to assess the accuracy of the obtained estimate, in terms of its standard deviation or its variance. To apply the bootstrap for variance estimation in system identification, and with specific reference to the problem of evaluating the standard deviation for the frequency response of the estimated model, the so-called method of bootstrapping residuals is used, which can be synthesized as follows:

1. Estimate the linear model $[\hat{A}, \hat{B}, \hat{C}, \hat{D}, \hat{K}]$ from the available input/output data (u, y) and compute the estimate for the points of interest of its frequency response $\hat{G}(j\omega_k)$, $k = 1, \ldots, N$.

2. Compute $e(t) = y(t) - \hat{y}(t)$.

3. Obtain an estimate $\hat{F}_e$ for the distribution F_e of the prediction error. In this work a parametric estimate will be considered and the normality assumption for the distribution of $e(t)$ will be made.

4. Generate B replications $(u^{*(i)}, y^{*(i)})$ of the original data set (u, y), with $u^{*(i)} = u$ and $y^{*(i)}$ obtained by feeding the identified model $[\hat{A}, \hat{B}, \hat{C}, \hat{D}, \hat{K}]$ with the deterministic input $u^{*(i)} = u$ and the stochastic input $e^{*(i)}$, $i = 1, \ldots, B$ where $e^{*(i)}$ is constructed by resampling (with replacement) from the distribution $\hat{F}_e$.

5. Estimate B replications of the identified model and of the points of interest for the frequency response $\hat{G}^{*(i)}(j\omega_k)$, $k = 1, \ldots, N$.

6. The estimate of the standard error for the frequency response of the model is finally given by:
(4)
$$\hat{\sigma}^*_{\hat{G}(j\omega_k)} = \frac{1}{\sqrt{B-1}} \left(\sum_{i=1}^{B} (\hat{G}^{*(i)}(j\omega_k) - \bar{\hat{G}}^*(j\omega_k))^2\right)^{\frac{1}{2}}$$
where
(5)
$$\bar{\hat{G}}^*(j\omega_k) = \frac{1}{B} \sum_{i=1}^{B} \hat{G}^{*(i)}(j\omega_k).$$

In a similar way one can obtain estimates of the standard deviation for the poles and zeros of the estimated model, as will be illustrated in a numerical example in Section 6.1.

4. ANALYSIS OF BLACK-BOX MODELS

As mentioned in the Introduction, subspace model identification algorithms return black-box models in state-space form, so the state variables of the identified models cannot be given a physical interpretation. Therefore, the identified models should be analysed to check that they do not contain modes introduced by numerical artifacts. Such a verification is carried out in terms of classical modal analysis. In particular, modes are inspected with respect to the non-physical states and with respect to the components of the output vector, as the projection of the model's modes on the output can of course be given a direct physical interpretation. At this level, modes either acting at very high frequencies or not providing significant contributions to the input/output behaviour over the frequency range of interest are removed, by means of conventional model reduction techniques.

Similarly, the output equation of the identified model is inspected to check the elements of the direct feedthrough term D, which is returned by the identification procedure (unless it is modified to return $D = 0$) but which is likely to be non-physical. This analysis is simply carried out by comparing the frequency response function of the model with and without individual elements of the D matrix to inspect whether they provide a significant contribution to the input/output behaviour over the relevant range of frequencies.

A numerical example of analysis of a black-box state-space model for the dynamics of a Leonardo helicopter is presented in Section 6.2.

5. PHYSICAL INTERPRETATION OF BLACK-BOX MODELS

The issue of "'matching"' black-box MIMO state space models to parametric model structures as a way to bridge the gap between black-box and grey-box model identification (and possibly use black-box models as initial guesses for iterative grey-box methods) has been studied by many Authors in the system identification literature. A few solutions are available, either based on frequency-domain model matching[18] or on the explicit construction of the similarity transformation relating the black-box model to the grey-box model structure[19,20,21]. Such methods

however imply the solution of large-scale optimisation problems, which at the current state-of-the-art cannot yet handle the complexity of MIMO flight dynamics models.

As an alternative, a different approach is adopted herein, in which a state transformation is constructed such that the output variables have a one-to-one dependency on the state variables, *i.e.*, the output matrix is the identity matrix or a partition of the identity matrix.

By means of the above-described steps the initial black-box model given by

$$\dot{x} = Ax + Bu \tag{6}$$

$$y = Cx + Du \tag{7}$$

can be brought to the form

$$\dot{z}_1 = \hat{A}_{11} z_1 + \hat{A}_{12} z_2 + \hat{B}_1 u \tag{8}$$

$$\dot{z}_2 = \hat{A}_{21} z_1 + \hat{A}_{22} z_2 + \hat{B}_2 u \tag{9}$$

$$y = z_1, \tag{10}$$

in which the outputs coincide with z_1. The state-space realization of the system now has at least partial physical meaning, in the sense that the first states coincide with the outputs of the system. In the following the procedure to construct the similarity transformation is described.

Consider a LTI system

$$\dot{x} = Ax + Bu \tag{11}$$

$$y = Cx + Du \tag{12}$$

with state, input and output dimension respectively of n, m, p. The C matrix defines the output transformation. If $D = 0$ and $C = I$, then $y = x$, *i.e.*, the output coincides with the state.

In general C is not the identity matrix, nor is it square ($p \neq n$); still, if the i-th row of C is a vector made up of zeros and one of its elements is 1

$$C = [c_{i,j}], \qquad i = 1 \dots p, \qquad j = 1 \dots n \tag{13}$$

$$c_{i,k} = 1 \qquad k \in \{1 \dots n\} \tag{14}$$

$$c_{i,j} = 0 \qquad \forall j \neq k, j \in \{1 \dots n\} \tag{15}$$

then the i-th output of the system depends only on the k-th state variable (and coincides with it, if the i-th row of the D matrix is made up of zeros). The objective is to find a state transformation such that the C matrix of the (transformed) system is made up of rows consistent with equations (15). In order to do this, a two-step approach is employed:

1. a QR decomposition is applied to the C matrix and a first state transformation depending on the Q matrix of the decomposition is constructed;
2. by means of a second state transformation, depending on the R matrix, a system where the C matrix satisfies the requirements is eventually obtained.

The QR decomposition[22] is briefly introduced in the following. Consider a matrix

$$X = \begin{bmatrix} Q_1 & Q_2 \end{bmatrix} \begin{bmatrix} R \\ 0 \end{bmatrix} \tag{16}$$

where $X \in \mathbb{R}^{n \times p}$, $p < n$, $rank(X) = p$, $Q_1 \in \mathbb{R}^{n \times p}$, $Q_2 \in \mathbb{R}^{n \times (n-p)}$, $R \in \mathbb{R}^{p \times p}$. The matrices Q_1, Q_2 are made up of normalized, linearly independent column vectors and $Q_1^T Q_1 = I, \quad Q_2^T Q_2 = I, \quad Q_1^T Q_2 = 0$. R is upper triangular. Q_1 is a basis for $range(X)$. Given the matrix X, the QR decomposition algorithm computes $Q = \begin{bmatrix} Q_1 & Q_2 \end{bmatrix}$ and R.

5.1 State transformation: step 1

Consider now matrix C in equation (7), assume that $p < n$ and C is full rank (rank$(C) = p$), so that the nullspace of C has dimension $n-p$, and let $n_1 = p$ and $n_2 = n - p$. Then, the QR decomposition is applied to C^T to get

$$C^T = \begin{bmatrix} T_1^T & T_2^T \end{bmatrix} \begin{bmatrix} R \\ 0 \end{bmatrix} \tag{17}$$

which is equivalent to

$$C = \begin{bmatrix} R^T & 0 \end{bmatrix} \begin{bmatrix} T_1 \\ T_2 \end{bmatrix}. \tag{18}$$

Letting now

$$T = \begin{bmatrix} T_1 \\ T_2 \end{bmatrix}, \tag{19}$$

the T matrix can be used to perform the state transformation $q = Tx$ on the system in equation (12)

$$\dot{q} = \tilde{A} q + \tilde{B} u \tag{20}$$

$$y = \tilde{C} q + \tilde{D} u \tag{21}$$

where

$$\tilde{A} = TAT^{-1} \quad \tilde{B} = TB \tag{22}$$

$$\tilde{C} = CT^{-1} \quad \tilde{D} = D. \tag{23}$$

5.2 State transformation: step 2

In view of the similarity transformation T, the $\tilde{C}$ matrix has the following structure

$$\tilde{C} = \begin{bmatrix} R^T & 0 \end{bmatrix}, \tag{24}$$

i.e., it is made up by a lower triangular left block R^T of dimensions $[p \times n_1]$, and a right block of zeros of dimensions $[p \times n_2]$. This implies that the output y

depends only on the first n_1 components of the state vector q. Considering the partition of the state vector q given by

$$q = \begin{bmatrix} q_1 \\ q_2 \end{bmatrix} \quad q_1 \in \mathbb{R}^{n_1}, \quad q_2 \in \mathbb{R}^{n_2}, \tag{25}$$

and assuming for simplicity that $D = 0$ (the results hold in the general case $D \neq 0$), the output y is given by

$$y = \tilde{C}q = \begin{bmatrix} R^T & 0 \end{bmatrix} \left| \begin{matrix} q_1 \\ q_2 \end{matrix} \right| = R^T q_1. \tag{26}$$

Matrix R^T is square, invertible and lower triangular. It is then possible to apply another state transformation $z = \hat{T}q$, defined as

$$z = \hat{T}q = \begin{bmatrix} R^T & 0 \\ 0 & I \end{bmatrix} \begin{bmatrix} q_1 \\ q_2 \end{bmatrix} = \begin{bmatrix} z_1 \\ z_2 \end{bmatrix}. \tag{27}$$

Note that since the output does not depend on q_2, the lower part of $\hat{T}$ was chosen to be the identity matrix. The transformed system turns out to be

$$\dot{z} = \hat{A}z + \hat{B}u \tag{28}$$

$$y = \hat{C}z + \hat{D}u \tag{29}$$

where

$$\hat{A} = \hat{T}\tilde{A}\hat{T}^{-1} \quad \hat{B} = \hat{T}\tilde{B} \tag{30}$$

$$\hat{C} = \tilde{C}\hat{T}^{-1} \quad \hat{D} = D \tag{31}$$

and

$$\hat{T}^{-1} = \begin{bmatrix} (R^T)^{-1} & 0 \\ 0 & I \end{bmatrix}. \tag{32}$$

Hence

$$\hat{C} = \begin{bmatrix} R^T & 0 \end{bmatrix} \begin{bmatrix} (R^T)^{-1} & 0 \\ 0 & I \end{bmatrix} = \begin{bmatrix} I & 0 \end{bmatrix}, \tag{33}$$

so matrix $\hat{C}$ has the desired structure: the p outputs coincide with $z_1 = R^T q_1$. The state realization of the system of equation (29) now has physical meaning, in the sense that the first p states coincide with the outputs of the system; still the output is influenced by the input u through the matrix D.

A numerical example of application of the above-described procedure to a black-box state-space model from the literature is presented in Section 6.3.

6. RESULTS

6.1 Role of uncertainty in ADS-33E-PRF small amplitude bandwidth and phase delay analysis

This section illustrates the role of uncertainty modelling of an identified model in correctly classifying the Target Acquisition and Tracking (small amplitude) level of an aircraft, based on the guidelines in ADS-33E-PRF[23]. The ADS-33E-PRF defines two parameters that should be computed from flight tests to exploit the small-amplitude responses Level, *i.e.*, bandwidth ω_{BW} and τ_p. As is well known, bandwidth is indicative of the highest frequency at which the aircraft-pilot loop can be closed without threatening stability, *i.e.*, it is a measure of the frequency below which the aircraft can follow all pilot commands. Phase delay τ_p, on the other hand, can be considered as an equivalent time delay of a highly augmented aircraft.

According to ADS33E[23], ω_{BW} and τ_p shall be obtained from frequency responses as defined in Figure 1 and equation (34).

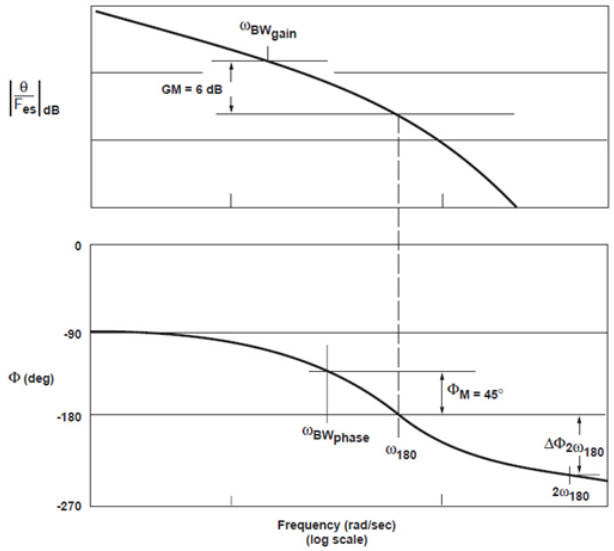

Figure 1: Definition of bandwidth ω_{BW} and phase delay τ_p.

$$\tau_p = \frac{\Phi(2\omega_{180}) - \Phi(\omega_{180})}{2\omega_{180}} \frac{\pi}{180}[s]. \tag{34}$$

To compute estimates of the frequency responses suitable datasets should be available, *e.g.*, responses to sweep signals. The execution of frequency sweeps however requires a significant amount of flight time. Moreover even if the nonparametric frequency response model is available, its reliability is a critical information. In this example the CT-PBSID black-box algorithm outlined in Section 2 is adopted, and the uncertainty of the identified model is estimated using a bootstrap approach, as discussed in Section 3. The idea is to identify a model of the closed-loop system, including AFCS, sensors and actuators dynamics, and helicopter dynamics, using pilot stick displacement as input and angular rate as output, as shown in Figure 2.

The proposed approach is time-domain based, therefore shorter and simpler input signals can be used, *e.g.*, doublets and 3211 sequences. The time histories obtained at the flight simulator are shown

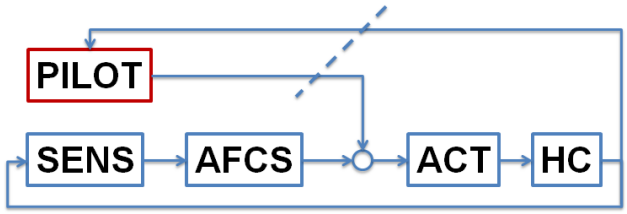

Figure 2: Input and output scheme for closed-loop model identification.

hereafter. The tests are two roll captures, but in the test B the pilot has been asked to accomplish the task in a shorter time and with smaller tolerance than test A. In particular, in the second test the actuator that reproduce the pilot maneuvering, reaches its maximum rate. In Figures 3 and 7 are shown the lateral cyclic stick movements for each of the two tests. It is evident that in the second case the pilot tries to adjust the overshoot (see Figure 8) reached due to the rate limiter that bounded the piloting speed maneuver, as shown in Figure 9.

In Figures 5 and 9 is shown a comparison between measured and simulated outputs, proving the capability of the identified models to capture the system dynamics.

Finally Figures 6 and 10 illustrate the bandwidth/phase delay plots for the two tests. As expected the test A, in which the rate limiter of the actuator has not been reached, exhibits better performance than test B. Of course without any information about the reliability of the identified models even the placement on the bandwidth/phase delay plot would be doubtful. In this simulated example it is already known that in the second case the rate limiter was relevant in the deterioration of both performance parameters, but with real flight data this conclusion might not be so straightforward. To manage this issue, the bootstrap-based approach outlined in Section 3 has been applied, so as to evaluate the uncertainty associated with the estiimated bandwidth and phase delay. The uncertainty estimation of the identified models, shown in Figures 6 and 10 as grey dots, suggest that in test A the real bandwidth and phase delay of the system are close to the identified ones, whilst in test B the real phase delay falls somewhere in the grey cloud and so it can be a bit far from the identified ones.

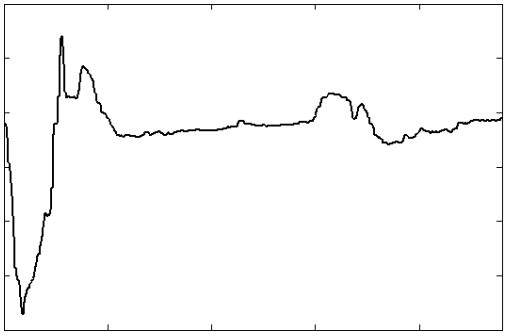

Figure 3: Test A: Lateral cyclic pilot input.

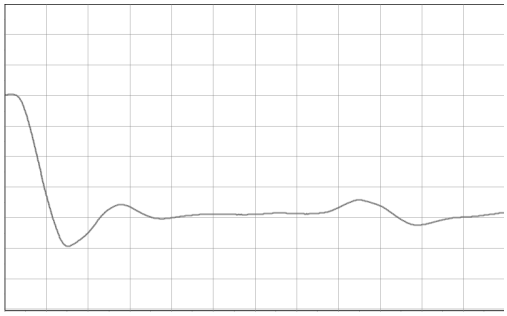

Figure 4: Test A: Roll angle.

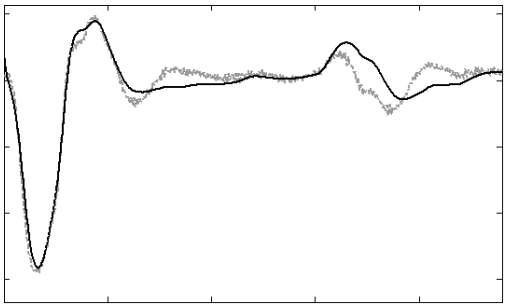

Figure 5: Test A: Roll rate (gray: measured, black: simulated).

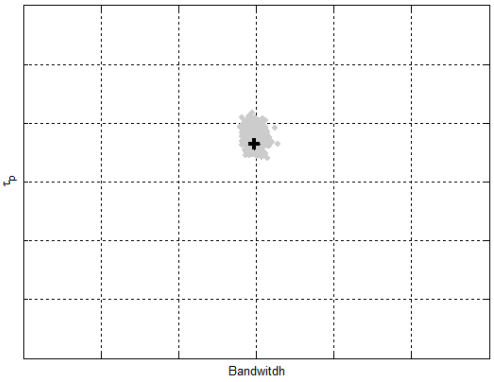

Figure 6: Test A: Bandwidth/Phase plot.

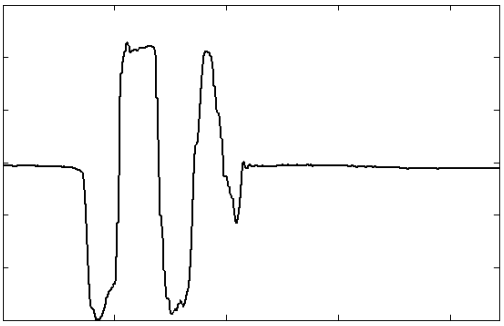

Figure 7: Test B: Lateral cyclic pilot input.

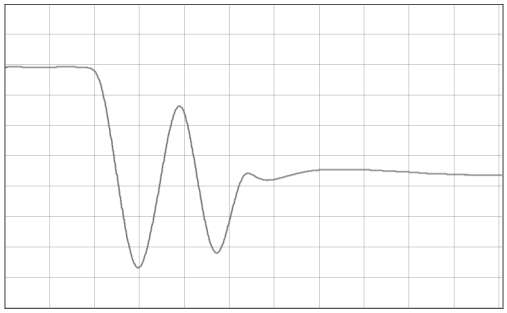

Figure 8: Test B: Roll angle.

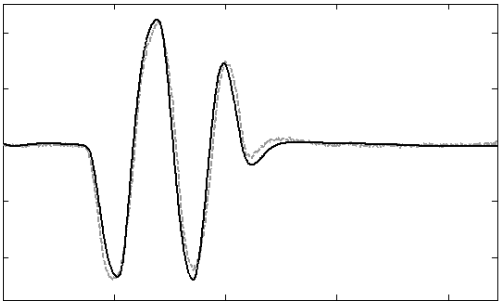

Figure 9: Test B: Roll rate (gray: measured, black: simulated).

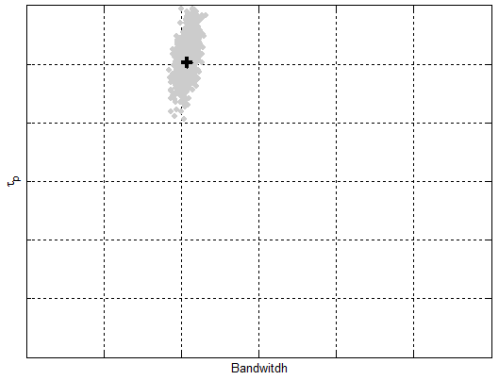

Figure 10: Test B: Bandwidth/Phase plot.

6.2 Modal decomposition and D-matrix analysis for a black-box helicopter model

As an example of the analysis procedure discussed in Section 4, modal contributions (*i.e.*, eigenvectors) were computed on an identified black-box model of a Leonardo helicopter and projected on the output space, which was restricted to the angular rates $[p, q, r]$ for this purpose. Modes have been labelled with letters and numerical values of the associated eigenvalues are not shown for confidentiality reasons. Normalized values of the modal contributions are shown in Table 1. The modal decomposition was then applied to the on-axis response of the pitch and roll axes in order to identify the dominant modal components related to such axes; these are shown in the last two columns of Table 1, respectively; Figures 11 and 12 show the modal decomposition plot for pitch and roll axes. It can be noticed that mode F indicates a strong participation of pitch rate; moreover, this mode does not dominate the response of the roll axis. On the other hand, it can be observed that modes D,E,G,H experience a small participation of pitch rate, despite being dominating modes in the pitch response.

Label	P	Q	R	Pitch	Roll
A	0.686	0.574	0.448		
B	0.577	0.113	0.809		
C	0.784	0.196	0.589		
D	0.956	0.118	0.269	X	X
E	0.883	0.337	0.326	X	X
F	0.039	0.987	0.157	X	
G	0.954	0.162	0.252	X	X
H	0.613	0.170	0.772	X	X
I	0.792	0.124	0.597		
J	0.952	0.095	0.290		

Table 1: Modal contributions projected on angular rate output variables.

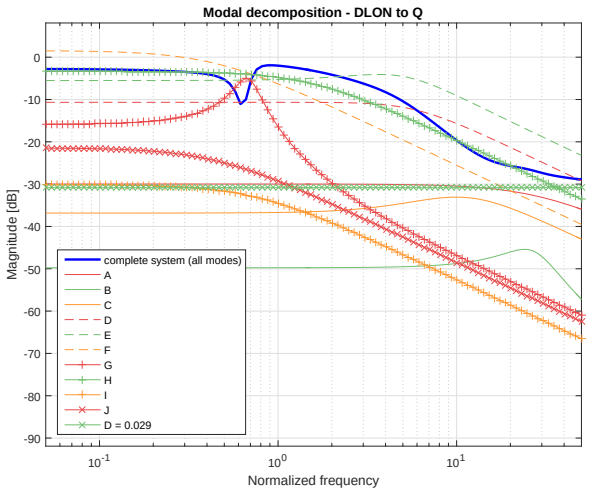

Figure 11: Modal decomposition, pitch axis.

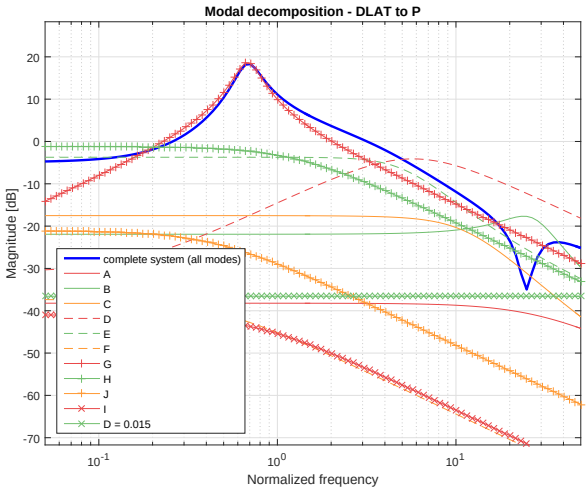

Figure 12: Modal decomposition, roll axis.

Similarly, the output equation is inspected to check the elements of the direct feed-through term D, which is returned by the identification procedure but which is likely to be non-physical. Analysis of the effect of the D term on the frequency response was carried out: the frequency response of the model transfer function obtained by imposing $D = 0$ was checked against the original one; normalized frequency responses of the transfer matrix on-axis terms related to pitch and roll axes are shown in Figures 13 and 14; the analysis indicates that the D term in the transfer matrix has little effect on the attitude dynamics in the frequency range of interest, thus can be neglected; indeed the feed-through term has an effect only at very high frequency. The other terms in the transfer matrix yield to similar conclusions and are not shown for brevity.

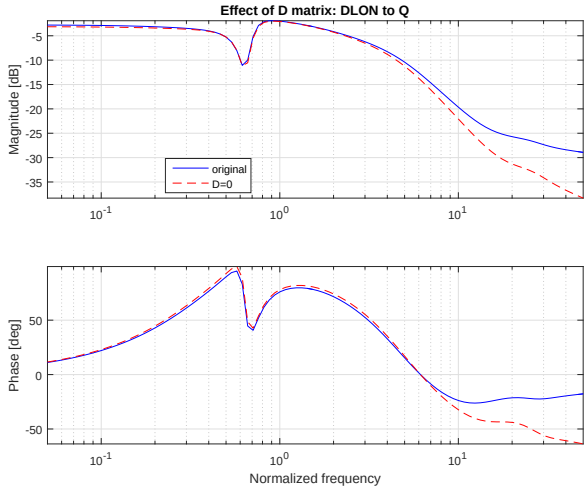

Figure 13: Effect of the D term on the frequency response of pitch axis.

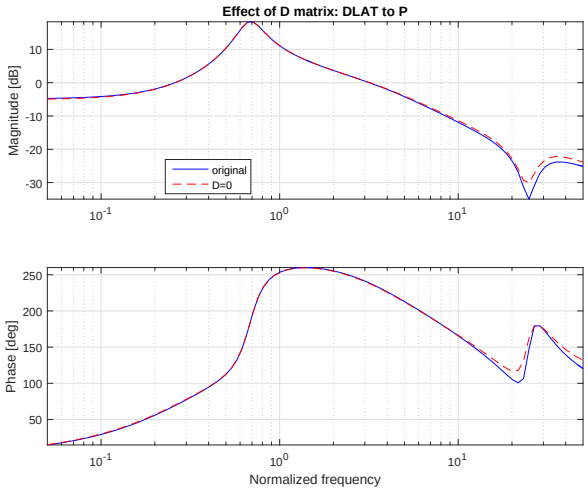

Figure 14: Effect of the D term on the frequency response of roll axis.

6.3 Change of coordinates for a black-box model

A numerical example is presented to show the potential of the state transformation approach presented in Section 5. The identified black-box model obtained in[24] is considered; the model is a discrete-time one, but the proposed state transformation applies to continuous-time as well as discrete-time models. The input vector is $u = [u_{roll}, u_{pitch}, u_{yaw}]^T$ and the output vector is $y = [\phi, \theta, \psi]^T$ (with respect to the model in[24] only the attitude output has been retained for this example). The state-space matrices of the original model are reported for convenience

$$A = \begin{bmatrix} 0.996 & 0 & 0.005 & -0.025 & -0.072 & 0.036 & 0.017 \\ -0.006 & 0.953 & 0.098 & -0.084 & -0.29 & 0.143 & 0.156 \\ -0.005 & -0.034 & 0.986 & 0.016 & 0.015 & 0 & -0.07 \\ -0.003 & 0.051 & 0.012 & 0.984 & 0.016 & -0.209 & 0.303 \\ 0.006 & 0.052 & 0.006 & 0 & 0.975 & 0.103 & -0.17 \\ 0.002 & -0.008 & 0.004 & 0.046 & -0.028 & 1.003 & 0.024 \\ 0.019 & 0.009 & -0.011 & 0.02 & 0.038 & 0.045 & 0.944 \end{bmatrix}$$

$$B = \begin{bmatrix} 0.027 & 0.005 & 0.004 \\ 0.072 & 0.087 & 0.022 \\ -0.005 & 0.016 & -0.007 \\ -0.029 & -0.083 & 0 \\ 0.023 & 0.014 & 0 \\ 0.007 & 0.018 & 0.002 \\ 0.032 & 0.112 & -0.002 \end{bmatrix}$$

$$C = \begin{bmatrix} -0.617 & -4.448 & -0.8 & 1.558 & 0.121 & -0.365 & -0.04 \\ 0.42 & 2.267 & -0.412 & 2.117 & -0.841 & -0.087 & 0.52 \\ -0.27 & -0.254 & -2.885 & -1.021 & -1.057 & -0.059 & 0.08 \end{bmatrix}$$

$$D = 0_{3\times 3}.$$

The states of the black-box model have no physical meaning and the C matrix is full rank. In order to partially recover physical meaning of the state variables, the state transformation given by the combination of equations (22) and (30) is applied. The similarity transformations T and $\hat{T}$ are respectively

$$T = \begin{bmatrix} -0.128 & -0.920 & -0.165 & 0.322 & 0.025 & -0.075 & -0.008 \\ -0.080 & -0.325 & 0.215 & -0.858 & 0.269 & 0.065 & -0.170 \\ -0.066 & 0.039 & -0.875 & -0.339 & -0.334 & -0.010 & 0.029 \\ 0.967 & -0.123 & -0.118 & -0.012 & 0.100 & 0.115 & -0.112 \\ -0.110 & 0.154 & -0.376 & 0.130 & 0.897 & -0.021 & 0.035 \\ -0.122 & -0.030 & -0.031 & 0.084 & -0.012 & 0.988 & 0.008 \\ 0.102 & -0.085 & 0.062 & -0.143 & 0.036 & 0.016 & 0.978 \end{bmatrix}$$

$$\hat{T} = \begin{bmatrix} 4.836 & 0 & 0 & 0 & 0 & 0 & 0 \\ -1.407 & -2.995 & 0 & 0 & 0 & 0 & 0 \\ 0.394 & 0.057 & 3.236 & 0 & 0 & 0 & 0 \\ 0 & 0 & 0 & 1 & 0 & 0 & 0 \\ 0 & 0 & 0 & 0 & 1 & 0 & 0 \\ 0 & 0 & 0 & 0 & 0 & 1 & 0 \\ 0 & 0 & 0 & 0 & 0 & 0 & 1 \end{bmatrix}.$$

The resulting state-space matrices in the transformed state-space system are given by

$$\hat{A} = \begin{bmatrix} 1.015 & 0.048 & -0.059 & 0.076 & 1.471 & -0.953 & -0.263 \\ -0.014 & 1.037 & 0.033 & -0.246 & -0.634 & -0.172 & 1.142 \\ -0.003 & -0.006 & 0.995 & 0.026 & 0.058 & 0.059 & 0.026 \\ -0.004 & 0.001 & 0.007 & 0.994 & -0.040 & 0.025 & -0.007 \\ -0.015 & -0.001 & 0.001 & 0.008 & 0.937 & 0.079 & -0.066 \\ 0.009 & 0.018 & -0.004 & -0.007 & -0.001 & 0.981 & 0.038 \\ 0.000 & -0.002 & -0.004 & 0.046 & 0.051 & 0.067 & 0.882 \end{bmatrix}$$

$$\hat{B} = \begin{bmatrix} -0.379 & -0.542 & -0.095 \\ 0.112 & 0.062 & 0.053 \\ -0.004 & 0.008 & 0.013 \\ 0.018 & -0.016 & 0.002 \\ 0.028 & 0.012 & 0.005 \\ -0.001 & 0.008 & 0.001 \\ 0.033 & 0.116 & -0.004 \end{bmatrix}$$

$$\hat{C} = \begin{bmatrix} 1 & 0 & 0 & 0 & 0 & 0 & 0 \\ 0 & 1 & 0 & 0 & 0 & 0 & 0 \\ 0 & 0 & 1 & 0 & 0 & 0 & 0 \end{bmatrix}$$

$$\hat{D} = D.$$

In this way, the first three components of the (transformed) state vector coincide with the outputs $[\phi, \theta, \psi]^T$.

7. CONCLUDING REMARKS

The use of black-box state-space models has a number of advantages in terms of the ability to capture the dynamics of the underlying system in an accurate way, comes with a number of issues, which have to be addressed to successfully employ them in the control design toolchain, namely the definition of model uncertainty, the analysis of the contribution of the individual modes to the input/output behaviour and the possibility to recover some physical insight from the black-box model. Approaches to handle each of these issues have been discussed and illustrated with numerical examples, which allow to conclude that, up to some post-processing, black-box state-space models can be effectively used for control-oriented purposes not unlike physical models and grey-box models.

REFERENCES

[1] M. Tischler and R. Remple. *Aircraft And Rotorcraft System Identification: Engineering Methods With Flight-test Examples*. AIAA, 2006.

[2] R. Jategaonkar. *Flight Vehicle System Identification*. AIAA, 2006.

[3] M. Bergamasco, A. Ragazzi, and M. Lovera. Rotorcraft system identification: a time/frequency domain approach. In *19th IFAC World Congress, Cape Town, South Africa*, 2014.

[4] M. Bergamasco and M. Lovera. Continuous-time predictor-based subspace identification using Laguerre filters. *IET Control Theory and Applications*, 5(7):856–867, 5 2011.

[5] G. van der Veen, J. W. van Wingerden, Bergamasco M., Lovera M., and M. Verhaegen. Closed-loop subspace identification methods: an overview. *IET Control Theory and Applications*, 7(10):1339–1358, 2013.

[6] M. Bergamasco and M. Lovera. Rotorcraft model identification: a black-box time/frequency domain approach. In *43rd European Rotorcraft Forum, Milano, Italy (submitted)*, 2017.

[7] J. W. van Wingerden. The asymptotic variance of the $PBSID_{opt}$ algorithm. In *16th IFAC Symposium on System Identification, Brussels, Belgium*, 2012.

[8] M. Bergamasco, M. Lovera, and Y. Ohta. Bootstrap-based model uncertainty assessment in continuous-time subspace model identification. In *52th IEEE Conference on Decision and Control (CDC)*, pages 5840 – 5845, Florence, Italy, 2013.

[9] M. Gevers. A personal view of the development of system identification: a 30-year journey through an exciting field. *IEEE Control Systems Magazine*, 26(6):93–105, 2006.

[10] R. Guidorzi. Canonical structures in the identification of multivariable systems. *Automatica*, 11(4):361–374, 1975.

[11] P. Van Overschee and B. De Moor. *Subspace identification: theory, implementation, application*. Kluwer Academic Publishers, 1996.

[12] M. Verhaegen and V. Verdult. *Filtering and System Identification: A Least Squares Approach*. Cambridge University Press, 2007.

[13] R. Johansson, M. Verhaegen, and C.T. Chou. Stochastic theory of continuous-time state-space identification. *IEEE Transactions on Signal Processing*, 47(1):41–51, 1999.

[14] B. R. J. Haverkamp. *State space identification: theory and practice*. PhD thesis, Delft University of Technology, 2001.

[15] V. Klein and E.A. Morelli. *Aircraft System Identification: Theory And Practice*. AIAA, 2006.

[16] A. Chiuso and G. Picci. Consistency analysis of certain closed-loop subspace identification methods. *Automatica*, 41(3):377–391, 2005.

[17] S. Bittanti and M. Lovera. Bootstrap-based estimates of uncertainty in subspace identification methods. *Automatica*, 36(11):1605–1615, 2000.

[18] M. Bergamasco and Lovera. State space model identification: from unstructured to structured models with an H_∞ approach. In *5th IFAC Symposium on System Structure and Control*, Grenoble, France, 2013.

[19] L. Xie and L. Ljung. Estimate physical parameters by black box modeling. In *Chinese Control Conference, Hangzhou, China*, 2002.

[20] P. Parrilo and L. Ljung. Initialization of physical parameter estimates. In *13th IFAC Symposium on System Identification, Rotterdam, The Netherlands*, 2003.

[21] O. Prot, G. Mercère, and J. Ramos. A null-space-based technique for the estimation of linear-time invariant structured state-space representations. In *16th IFAC Symposium on System Identification, Brussels, Belgium*, 2012.

[22] S. Boyd and L. Vandenberghe. *Convex Optimization*. Cambridge University Press, 2004.

[23] ADS-33E-PRF. *Aeronautical Design Standard, Handling Qualities Requirements for Military Rotorcraft*. U.S. Army Aviation and Missile Command, Huntsville, Alabama, 2000.

[24] C. Chen, L. Shen, D. Zhang, and J. Zhang. Subspace-based system identification for a hovering tiltrotor UAV attitude dynamics. In *28th Chinese Control and Decision Conference (CCDC)*, 2016.